The influence of vehicles on the flutter stability of a long-span suspension bridge

Yan Han[1a], Shuqian Liu[1], C.S. Cai[*2], Jianren Zhang[1], Suren Chen[3] and Xuhui He[4]

[1]*School of Civil Engineering and Architecture, Changsha University of Science & Technology, Changsha, China, 410004*
[2]*Department of Civil and Environmental Engineering, Louisiana State University, Baton Rouge, USA, LA 70803*
[3]*Department of Civil and Environmental Engineering, Colorado State University, Fort Collins, USA, Co 80523*
[4]*School of Civil Engineering, Central South University, Changsha, China, 410075*

Abstract. The presence of traffic on a slender long-span bridge deck will modify the cross-section profile of the bridge, which may influence the flutter derivatives and in turn, the critical flutter wind velocity of the bridge. Studies on the influence of vehicles on the flutter derivatives and the critical flutter wind velocity of bridges are rather rare as compared to the investigations on the coupled buffeting vibration of the wind-vehicle-bridge system. A typical streamlined cross-section for long-span bridges is adopted for both experimental and analytical studies. The scaled bridge section model with vehicle models distributed on the bridge deck considering different traffic flow scenarios has been tested in the wind tunnel. The flutter derivatives of the modified bridge cross section have been identified using forced vibration method and the results suggest that the influence of vehicles on the flutter derivatives of the typical streamlined cross-section cannot be ignored. Based on the identified flutter derivatives, the influence of vehicles on the flutter stability of the bridge is investigated. The results show that the effect of vehicles on the flutter wind velocity is obvious.

Keywords: long-span suspension bridges; flutter stability; influence of vehicles; finite element (FE) model; ANSYS

1. Introduction

Compared to those bridges with shorter spans, long-span suspension bridges are more flexible and slender. These long-span bridges are thus more susceptible to flutter, which is a self-induced periodical motion with divergent amplitudes leading to the destruction of the structure. The research on the flutter stability of long-span bridges is crucial to the bridge safety and becomes one of the key issues in bridge wind engineering (Scanlan 1978).

Flutter analysis is to evaluate the lowest critical flutter wind speed as well as the corresponding flutter frequency in either the frequency or time domain. Several methods have been proposed for

---

∗Corresponding author, Professor, E-mail: cscai@lsu.edu
[a] Associate Professor, E-mail: ce_hanyan@163.com

the flutter analysis of bridges, such as the full-order flutter analysis method (Miyata and Yamada 1990, Dung *et al*. 1998, Ge and Tanaka 2000, Ding et al. 2002), the multimode flutter analysis technique (Xie and Xiang 1985; Agar 1989; Namini *et al*. 1992, Tanaka *et al*. 1992, Jain *et al*. 1996, Cai *et al*. 1999, Katsuchi *et al*. 1999, Zhang and Sun 2004, Chen 2007, Hua *et al*. 2007), etc. In traditional flutter analysis, vehicles were typically ignored in the identification of the flutter derivatives and the numerical predictions mainly because it was believed that the traffic would be closed under strong wind. With the increase of bridge span, flutter instability may occur at the fairly low wind speed because of the large flexibility and low structural damping (Scanlan and Tomko 1971, Scanlan and Jones 1990). Moreover, the traffic has rarely been closed even when preset wind speed limit is reached, considering the significant economy consequence and impact on the local transportation. Therefore, vehicles and strong wind effects may appear on long-span bridges at the same time (Chen *et al*. 2009). Consequently, if the traffic is realistically considered, the aerodynamic configuration of the bridge cross section will be modified. Therefore, it becomes instrumental to investigate the effect of vehicles on the flutter derivatives and the flutter instability of long-span bridges.

Traditional flutter stability analyses were typically conducted with some in-house FE packages developed specifically to tackle flutter analysis of bridges or through the aeroelastic wind tunnel tests, which are unavailable to the bridge design and management communities. An alternative way was to extend the commercial finite element (FE) packages such as ANSYS and ADINA to consider motion-dependent wind loads. In recent years, some successful efforts (Hua *et al*. 2007, Han 2007, Chen *et al*. 2009) have been made to carry out the flutter and buffeting analysis of long-span bridges with ANSYS.

Studies on the influence of vehicles on the flutter derivatives and the critical flutter wind velocity of bridges are rather rare as compared to the investigations on the coupled buffeting vibration of the wind-vehicle-bridge system (Cai and Chen 2004). This research program investigates the impact of vehicles on the aerodynamic derivatives and the flutter instability of a typical streamlined cross-section for long-span bridges. Firstly, the forced vibration device is adopted to carry out a series of wind tunnel tests to examine the flutter derivatives of the bridge considering the effect of the vehicles under different traffic flows. Secondly, flutter analysis is then performed with ANSYS (Hua *et al*. 2007, Han 2007, Chen *et al*. 2009) based on the experimentally determined flutter derivatives (Han et al. 2014). Finally, the effects of vehicles on the flutter stability of the bridge are investigated.

The wind tunnel experiments are outlined in Section 2, which illustrates the bridge deck and vehicle geometries, simulations of different traffic flows, testing conditions and procedure, and the identified flutter derivatives. Section 3 describes the methodology of flutter stability analysis using ANSYS. The flutter stability of the bridge and the effects of vehicles on the bridge are discussed in Section 4. Finally, some conclusions are drawn in Section 5. It is found that the effects of vehicles on the flutter derivatives and the flutter stability are all obvious.

2. Wind tunnel experiments of flutter derivatives under different traffic flows

2.1 The streamlined cross-section and vehicle model in wind tunnel

To provide general insights for most long-span bridges, a typical streamlined cross section for a long-span suspension bridge is selected for the investigation. The bridge section model has a 1:60

scale and the length of the model is 1.50 m. Two vehicle types, a sedan and a big passenger car, are considered in this study and the models are made with cystosepiments to reduce the weight. The widths of the sedan and the big passenger car are 2.88 cm and 3.67 cm, respectively. The details and dimensions of the bridge deck section and the vehicles are given in Figs. 1(a)-1(c).

2.2 Simulated traffic flow and testing cases

There are six levels of service from A to F according to the highway capacity manual (Chen and Wu 2011, Han *et al.* 2014). In the present study, a number of stationary vehicle models are placed on the bridge section model which replicates three kinds of traffic flow scenarios ─ free flow, moderate flow and busy flow corresponding to level B (9 vehicles/km/lane), level D (20 vehicles/km/lane) and level F (32 vehicles/km/lane), respectively. Traffic flow through the bridge is stochastic and there are many kinds of vehicle distributions. For the sensitivity analysis of the vehicle distributions on the bridge deck, four kinds of vehicle arrangements are considered for each traffic flow in this study. The proportions of the vehicles in category 1 (sedan) and 2 (big passenger car) among all vehicles are assumed to be 0.7 and 0.3, respectively. There are totally 8 lanes in the two traffic directions and the simulated traffic flows are shown in Fig. 2.
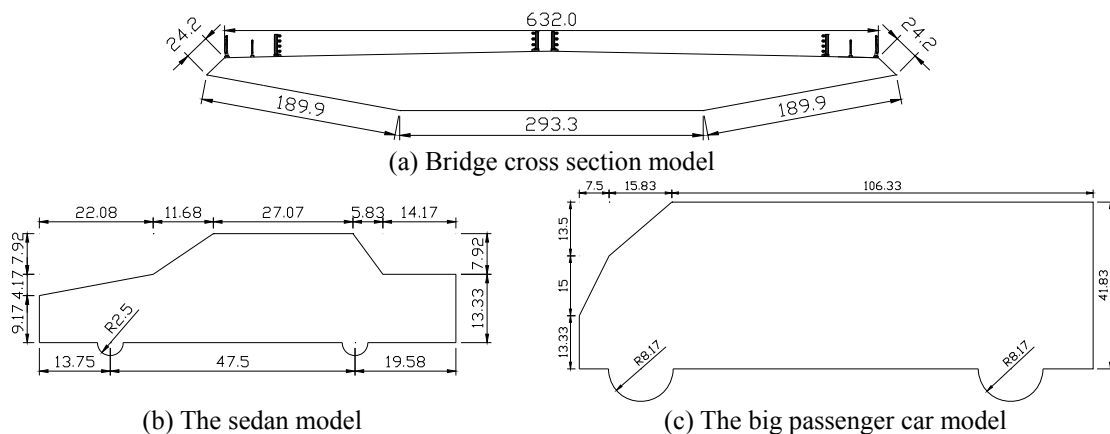

(a) Bridge cross section model

(b) The sedan model   (c) The big passenger car model

Fig. 1 Model geometry and overall dimensions (Unit: mm)

Table 1 Testing cases

Case	Traffic flow	Wind field	Wind attack angle (degree)	Arrangements
1	Free flow	Smooth	-3, 0, 3	1, 2, 3, 4
2	Moderate flow	Smooth	-3, 0, 3	1, 2, 3, 4
3	Busy flow	Smooth	-3, 0, 3	1, 2, 3, 4
4	No vehicle on the bridge	Smooth	-3, 0, 3	N.A.

A series of wind tunnel tests were carried out based on the forced vibration device (Han *et al.* 2014, Niu *et al.* 2007, 2011) in the HD-2 wind tunnel at Hunan University, China, which is a low-speed, one-circuit medium-sized boundary layer wind tunnel with two parallel test sections. Three wind attack angles of -3°, 0°, and $+3^{\circ}$ were investigated and the experimental configurations examined in the current work are outlined in Table 1.
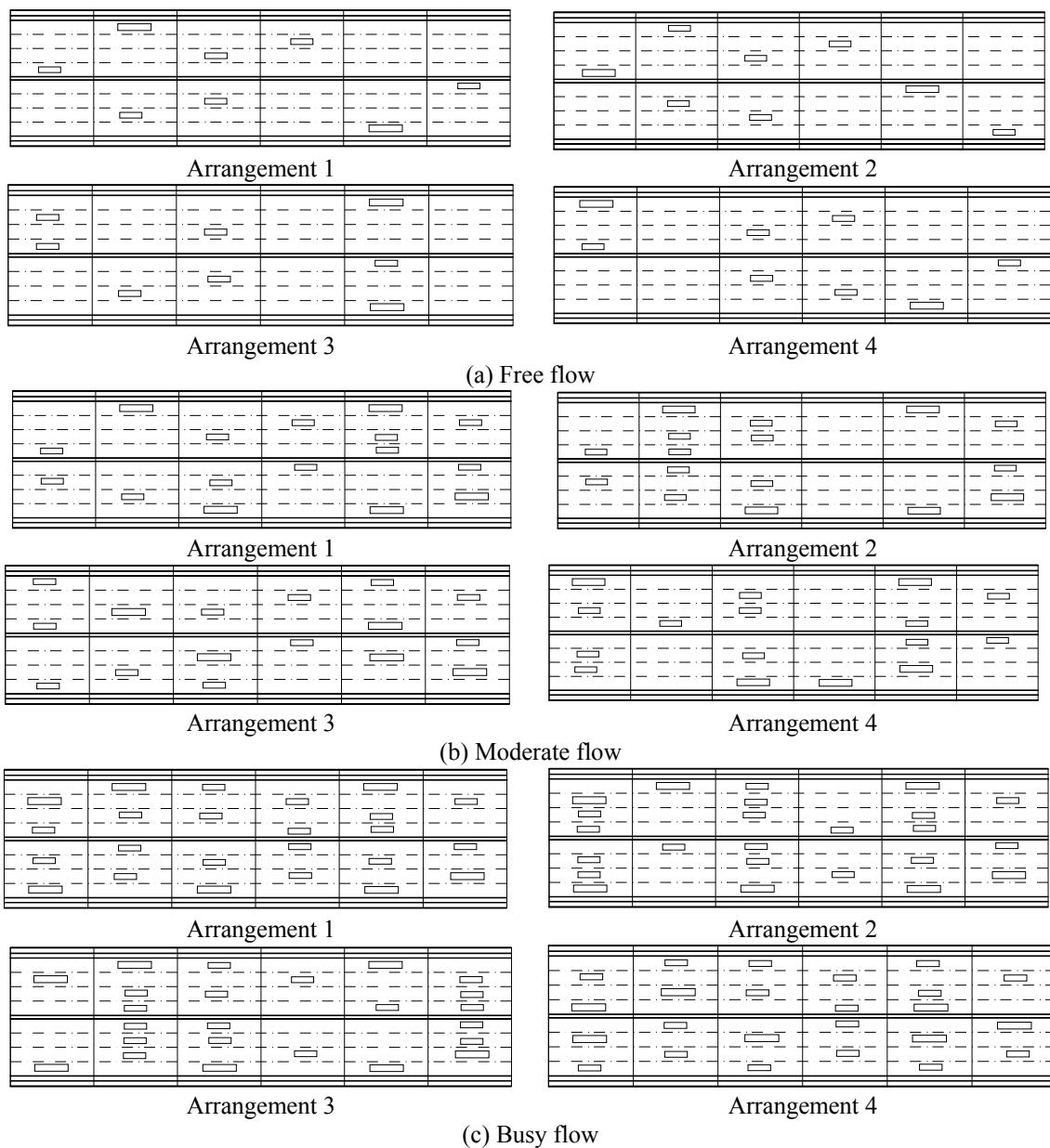

Arrangement 1   Arrangement 2

Arrangement 3   Arrangement 4

(a) Free flow

Arrangement 1   Arrangement 2

Arrangement 3   Arrangement 4

(b) Moderate flow

Arrangement 1   Arrangement 2

Arrangement 3   Arrangement 4

(c) Busy flow

Fig. 2 Simulated traffic flow (▭ the big passenger car; ▭ the sedan)

2.3 Identification results of flutter derivatives and discussions

The time-domain forced vibration method was used to identify the flutter derivatives of the bridge (Han *et al.* 2014). Figs. 3-10 illustrate the eight aerodynamic derivatives versus the reduced wind speed (=$U/(f.B)$) for Arrangement-1. In these figures, f_h and f_t are the frequencies in the vertical and torsional directions, respectively. It can be seen that the influences of vehicles under different traffic flows on the aerodynamic derivatives A_2^*, A_4^*, H_2^* and H_4^* for all considered wind attack angles are more obvious. However, there is only small influence on the aerodynamic derivatives A_1^* and A_3^* mainly for the high reduced wind speeds, and almost no influence on the aerodynamic derivative H_3^*. The reason may be that the values of A_2^*, A_4^*, H_2^* and H_4^* are relatively small and sensitive to the disturbance from experimental errors or other factors. On the contrary, the values of H_3^* are relatively large and less susceptible to the disturbance.
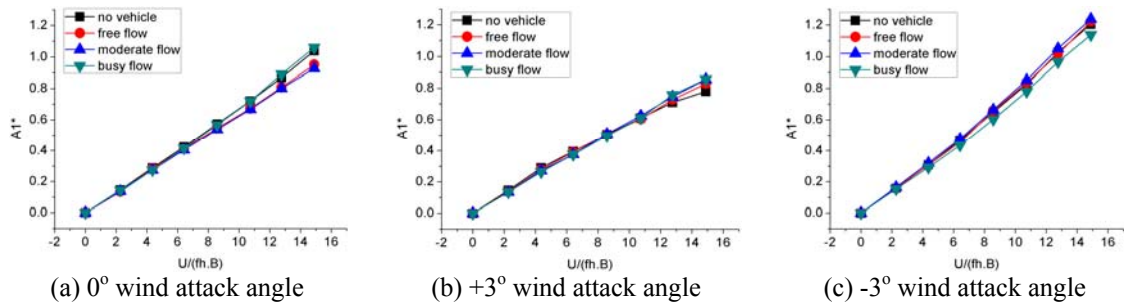

(a) 0° wind attack angle   (b) +3° wind attack angle   (c) -3° wind attack angle

Fig. 3 Aerodynamic derivatives A_1^* vs. reduced wind speed for different wind attack angles

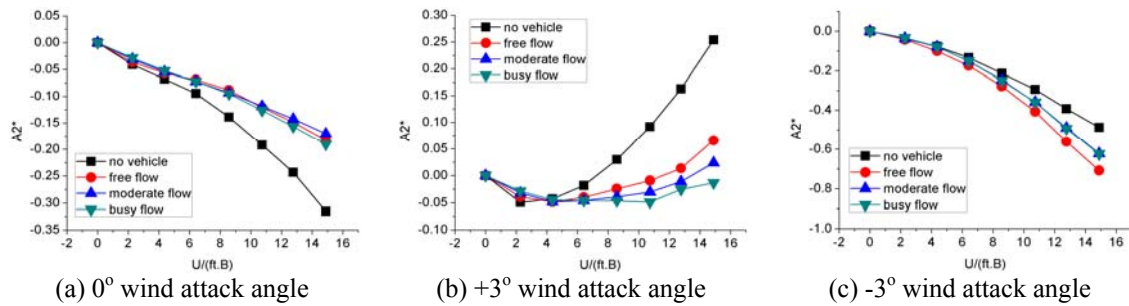(a) 0° wind attack angle   (b) +3° wind attack angle   (c) -3° wind attack angle

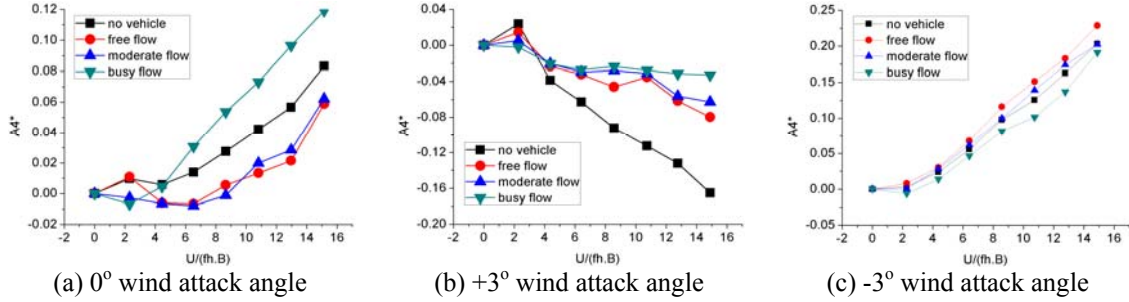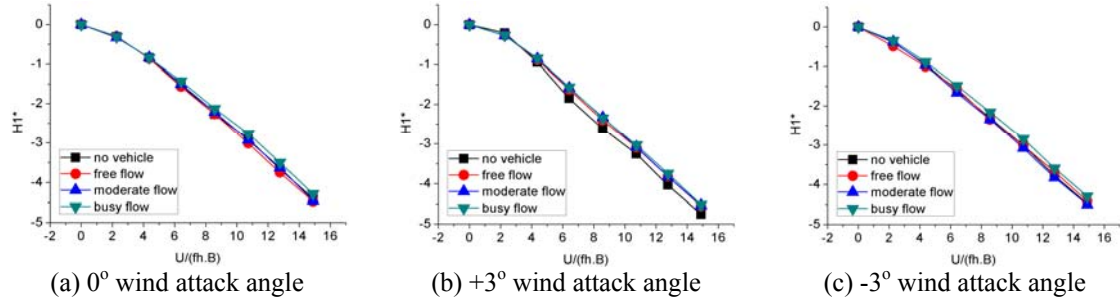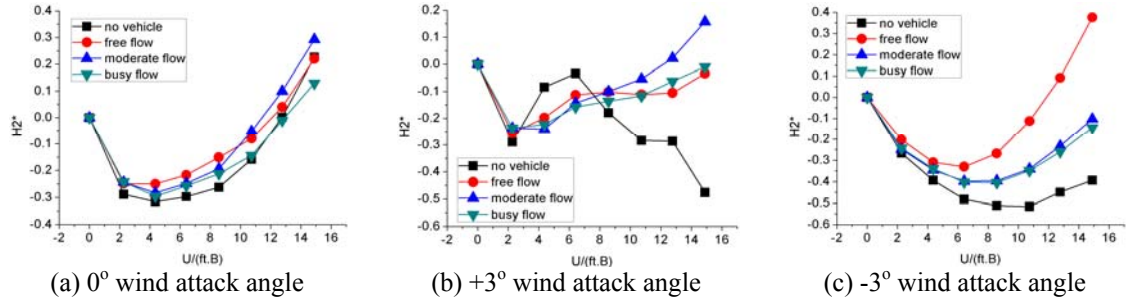Fig. 4 Aerodynamic derivatives A_2^* vs. reduced wind speed for different wind attack angles

(a) 0° wind attack angle   (b) +3° wind attack angle   (c) -3° wind attack angle

Fig. 5 Aerodynamic derivatives A_3^* vs. reduced wind speed for different wind attack angles

(a) 0° wind attack angle (b) +3° wind attack angle (c) -3° wind attack angle

Fig. 6 Aerodynamic derivatives A^*_4 vs. reduced wind speed for different wind attack angles

(a) 0° wind attack angle (b) +3° wind attack angle (c) -3° wind attack angle

Fig. 7 Aerodynamic derivatives H^*_1 vs. reduced wind speed for different wind attack angles

(a) 0° wind attack angle (b) +3° wind attack angle (c) -3° wind attack angle

Fig. 8 Aerodynamic derivatives H^*_2 vs. reduced wind speed for different wind attack angles

(a) 0° wind attack angle (b) +3° wind attack angle (c) -3° wind attack angle

Fig. 9 Aerodynamic derivatives H^*_3 vs. reduced wind speed for different wind attack angles

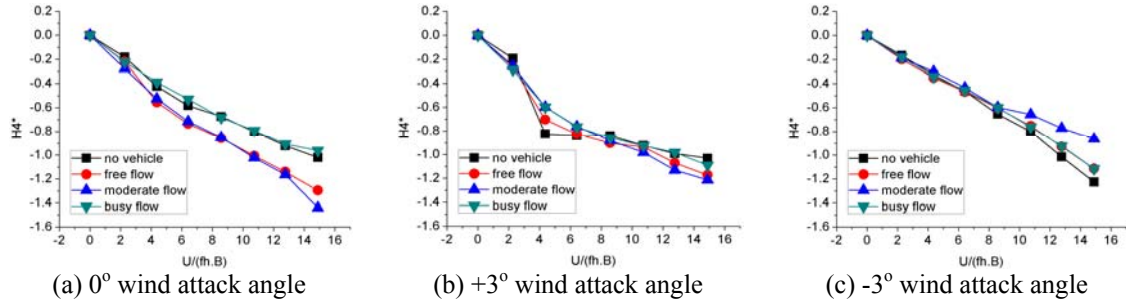(a) 0° wind attack angle   (b) +3° wind attack angle   (c) -3° wind attack angle

Fig. 10 Aerodynamic derivatives H_4^* vs. reduced wind speed for different wind attack angles

The aerodynamic derivative A_2^* is the wind coefficient that significantly influences the aerodynamic damping of the torsional vibration, which is usually critical to the flutter stability of streamlined cross sections. Negative A_2^* represents positive aerodynamic damping and positive for negative aerodynamic damping. From Fig. 4, it can be seen that A_2^* is negative at the 0° and -3° attack angles, and positive at +3° attack angle. At the 0° attack angle, the presence of vehicles under different traffic flow conditions all reduces the positive damping, while increases the positive damping at the -3° attack angle. At the +3° attack angle, the presence of vehicles reduces the negative damping. It is apparent that the presence of vehicles at the 0° attack angle has adverse impact on the aerodynamic stability of the bridge, while with favorable impacts at +3° and -3° attack angles.

The aerodynamic derivative A_2^* is usually sensitive to the presence of vehicles, as shown in Fig. 4. Thus, the sensitivity analysis of the vehicle distribution on A_2^* is conducted in this study. Figs. 11-13 show the direct aerodynamic derivative A_2^* for the four arrangements of vehicles on the bridge deck under the three traffic flow conditions. As shown in Figs. 11-13, vehicle distribution is found to have little influence on the flutter derivatives. Thus, one of the four arrangements of vehicles on the bridge deck can be selected to represent the vehicle distributions for each traffic flow scenario. Specifically, in the following studies, the flutter derivatives of Arrangement-1 are adopted.
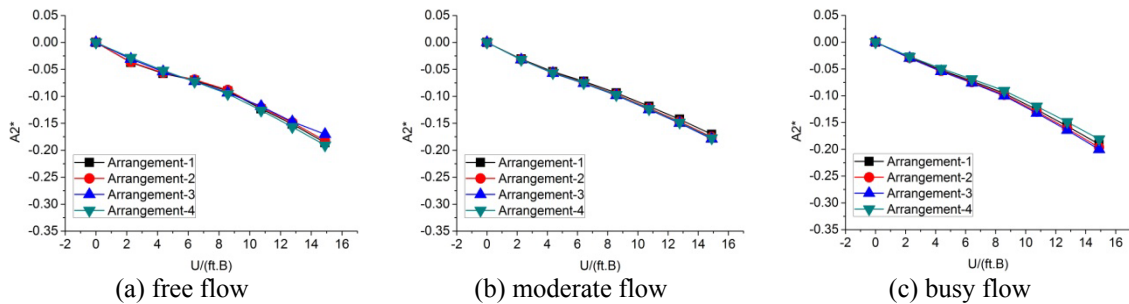

(a) free flow   (b) moderate flow   (c) busy flow

Fig. 11 Aerodynamic derivatives A_2^* vs. reduced wind speed under different traffic flows at 0° wind attack angles
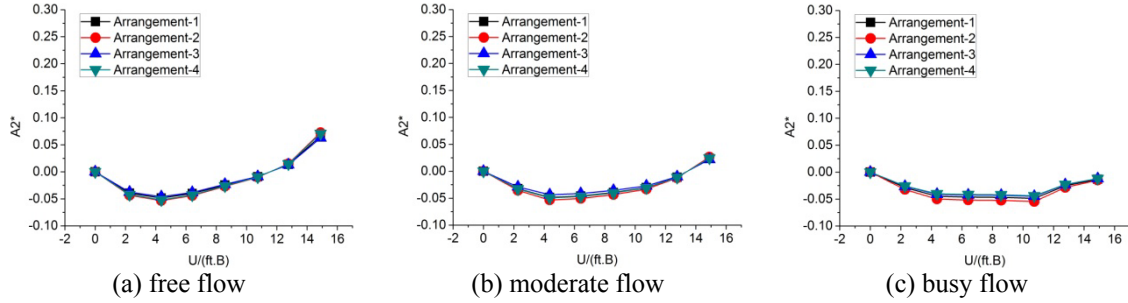
Fig. 12 Aerodynamic derivatives A^*_2 vs. reduced wind speed under different traffic flows at $+3^o$ wind attack angles
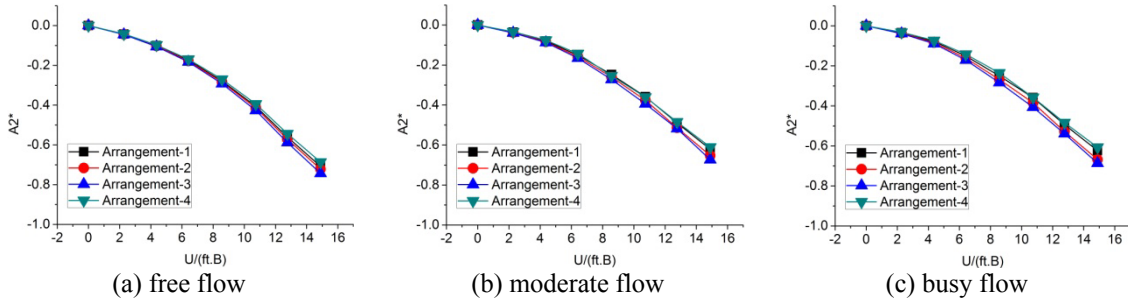

Fig. 13 Aerodynamic derivatives A^*_2 vs. reduced wind speed under different traffic flows at -3° wind attack angles

3. Aerodynamic stability analysis using ANSYS

The bridge motion equations in smooth flow can be expressed as

$$\mathbf{M\ddot{q} + C\dot{q} + Kq = F}_{se} \tag{1}$$

where $\mathbf{M}$, $\mathbf{C}$ and $\mathbf{K}$ are the global mass, damping and stiffness matrices, respectively; $\mathbf{q}$, $\mathbf{\dot{q}}$ and $\mathbf{\ddot{q}}$ represent the nodal displacement, velocity and acceleration vectors, respectively; and $\mathbf{F}_{se}$ denotes the vector of the nodal aeroelastic forces.

In the finite element analysis, after the distributed wind forces are converted into equivalent nodal loadings acting at the element nodes, the aeroelastic forces for element e can be expressed in terms of nodal displacement and nodal velocity as

$$\mathbf{F}^e_{ae} = \mathbf{K}^e_{ae}\mathbf{q}^e + \mathbf{C}^e_{ae}\mathbf{\dot{q}}^e \tag{2}$$

where $\mathbf{K}^e_{ae}$ and $\mathbf{C}^e_{ae}$ represent the local aeroelastic stiffness and damping matrices for element e, respectively; and $\mathsf{q}^e = \{q_1 \quad q_2 \quad ... \quad q_{12}\}^T$ is the displacement vector of element e. Similar to the general procedures in formulating element mass matrix, either a lumped or consistent formulation can be used to derive the element aeroelastic stiffness and damping matrices (Namini 1991). Chen

and Han (2007) found that the flutter limit speed obtained by using the lumped formulation is lower than that by using the consistent formulation, which is more conservative from engineering perspective. In this study, the lumped formulation is therefore adopted and the matrices of $\mathbf{K}^e_{ae}$ and $\mathbf{C}^e_{ae}$ are expressed as

$$\mathbf{K}^e_{ae} = \begin{bmatrix} \mathbf{K}^e_{ae1} & 0 \\ 0 & \mathbf{K}^e_{ae1} \end{bmatrix}, \qquad \mathbf{C}^e_{ae} = \begin{bmatrix} \mathbf{C}^e_{ae1} & 0 \\ 0 & \mathbf{C}^e_{ae1} \end{bmatrix} \tag{3}$$

in which

$$\mathbf{K}^e_{ae1} = a \begin{bmatrix} 0 & 0 & 0 & 0 & 0 & 0 \\ 0 & P_4^* & P_6^* & BP_3^* & 0 & 0 \\ 0 & H_6^* & H_4^* & BH_3^* & 0 & 0 \\ 0 & BA_6^* & BA_4^* & B^2 A_3^* & 0 & 0 \\ 0 & 0 & 0 & 0 & 0 & 0 \\ 0 & 0 & 0 & 0 & 0 & 0 \end{bmatrix}, \quad \mathbf{C}^e_{ae1} = b \begin{bmatrix} 0 & 0 & 0 & 0 & 0 & 0 \\ 0 & P_1^* & P_5^* & BP_2^* & 0 & 0 \\ 0 & H_5^* & H_1^* & BH_2^* & 0 & 0 \\ 0 & BA_5^* & BA_1^* & B^2 A_2^* & 0 & 0 \\ 0 & 0 & 0 & 0 & 0 & 0 \\ 0 & 0 & 0 & 0 & 0 & 0 \end{bmatrix} \tag{4}$$

where $a = \rho U^2 K^2 L_e / 2$ and $b = \rho U B K L_e / 2$; and L_e is the length of element e.

Hua *et al.* (2007) developed a hybrid finite element model that uses *Matrix27* to model the flutter-derivative-based aeroelastic forces in ANSYS, and used it for flutter analysis in the frequency domain. Two fictitious *Matrix27* models were integrated into the FE model to simulate the aeroelastic stiffness component and the aeroelastic damping component. Assembling all elemental matrices into global aeroelastic stiffness and damping matrices leads to

$$\mathbf{F}_{ae} = \mathbf{K}_{ae} \mathbf{q} + \mathbf{C}_{ae} \dot{\mathbf{q}} \tag{5}$$

where $\mathbf{K}_{ae}$ and $\mathbf{C}_{ae}$ denote the global aeroelastic stiffness and damping matrices, respectively.

Substituting Eq. (5) into Eq. (1) results in the governing equations of motion for the bridge as

$$\mathbf{M}\ddot{\mathbf{q}} + (\mathbf{C} - \mathbf{C}_{ae})\dot{\mathbf{q}} + (\mathbf{K} - \mathbf{K}_{ae})\mathbf{q} = \mathbf{0} \tag{6}$$

After incorporating the Rayleigh structural damping matrix assumption $\mathbf{C} = \alpha\mathbf{M} + \beta\mathbf{K}$, the governing equations of motion for flutter analysis becomes

$$\mathbf{M}\ddot{\mathbf{q}} + (\overline{\mathbf{C}} - \overline{\mathbf{C}}_{ae})\dot{\mathbf{q}} + (\mathbf{K} - \mathbf{K}_{ae})\mathbf{q} = \mathbf{0} \tag{7}$$

where $\overline{\mathbf{C}}$ is the modified damping matrix and $\overline{\mathbf{C}}_{ae}$ is the modified aeroelastic damping matrix and they are expressed as

$$\overline{\mathbf{C}} = \alpha\mathbf{M} + \beta(\mathbf{K} - \mathbf{K}_{ae}) \tag{8}$$

$$\overline{\mathbf{C}}_{ae} = \mathbf{C}_{ae} - \beta\mathbf{K}_{ae} \tag{9}$$

in which α and β are the proportionality coefficients for Rayleigh damping which can be obtained by least squares fitting, as

$$\min_{\alpha, \beta} \sum_{i=1}^{m} \left(2\xi_i \omega_i - \alpha - \beta \omega_i^2 \right)^2 \tag{10}$$

in which ξ_i is the damping ratio of the ith mode; and m is the total number of mode considered.

In this study, a mode-by-mode tracing method (Ge and Tanaka 2000) is adopted to iteratively search the flutter frequency and determine the critical flutter wind velocity. Making use of the tool APDL in ANSYS, the sweep and iterative procedure is implemented.

4. Modal analysis of the bridge

The long-span suspension bridge has a main span of 600 m and a streamlined steel box girder with a width of 36.9 m and a height of 3.5 m, as shown in Fig. 14, which is scaled by 1/60 as shown in Fig. 1(a). The two main cable planes are 26.7 m apart and the bridge deck is suspended by hangers at intervals of 12 m. The two bridge towers are reinforced concrete structures with a height of 112.7 m and 107.6 m, respectively. The material and sectional parameters of the bridge are shown in Table 2.

The initial FE model of the bridge is established using ANSYS, as shown in Fig. 15, with 521 elements. In the finite element model, the main girders and two towers are modeled by spatial beam elements with 6 degrees of freedom (DOF) at each node. The main cables and hangers are simulated as spatial truss elements with 3 DOFs at each node. The truss elements are tension-only, and the nonlinearity of the main cable stiffness due to the gravity is approximated by using the equivalent modulus of elasticity (Ernst 1965).
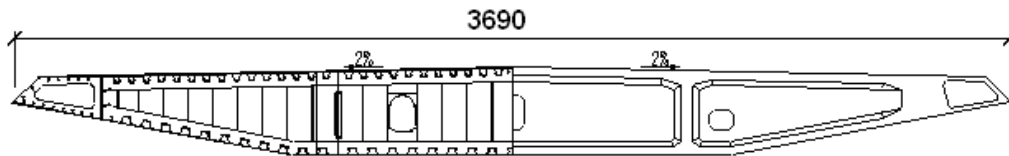

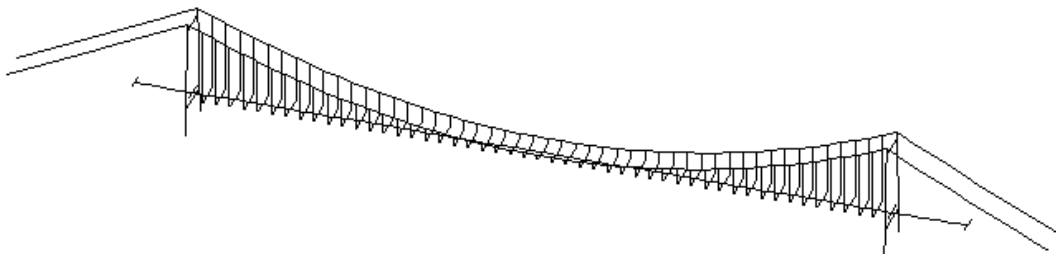Fig. 14 The cross section of the bridge (unit: mm)

Fig. 15 Initial FE model

Table 2 Material and sectional parameters of the bridge

Structural members	A (m^2)	J_θ (m^4)	J_y (m^4)	J_z (m^4)	E (GPa)	ρ (kg/m^3)
Main girder	1.31	5.13	1.93	102.00	210	15643
Main cables	0.1753	-	-	-	210	8000
Hangers	0.0031	-	-	-	210	8000
Towers	17.03-26.94	122.6-241.9	64.67-112.6	86.64-197.6	35	2650

Note: A-section area; J_θ-torsional moment of inertia; J_y-vertical bending moment of inertia; J_y-lateral bending moment of inertia; E- modulus of elasticity; ρ-density
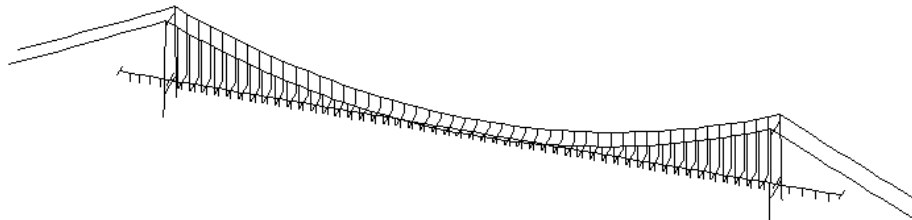

Fig. 16 FE model for flutter stability analysis

A series of *Matrix27* elements are integrated into the FE model to simulate the self-excited aerodynamic forces acting on the main girders. One end node is attached to the nodes of the main girder elements and the other end node of them is constrained. There are a total of 114 *Matrix27* elements, of which half modeling the aerodynamic stiffness and half modeling the aerodynamic damping. Fig. 16 shows the FE model of the bridge incorporating the Matrix27 elements for flutter stability analysis, where the boundary conditions for the constrained nodes are not displayed for clarity.

The dynamic characteristics of the bridge, including its natural vibration frequencies, vibration mode shapes, and mechanical damping properties are important factors that can significantly affect its flutter stability behavior. The first twenty natural modes are extracted using the Lanczos method in ANSYS, and the natural vibration frequencies and mode shapes of the first ten modes are summarized in Table 3. Some typical mode shapes are shown in Fig. 17.

The frequency of the fundamental mode is 0.1069 Hz, which is a floating mode in the longitudinal direction. This type of vibration mode is expected for the floating deck system. The vertical and torsional vibrations of the main girder of the bridge are usually critical for the flutter stability assessment of suspension bridges. For this particular bridge, the first modes of these two directions of motion (i.e., the third and eleventh modes) have the frequencies of 0.2442 Hz and 0.5758 Hz, respectively. The frequency ratio of these two modes is 2.36 and usually when the frequencies of the vertical mode and the torsional mode become closer, the possibility of interaction or coupling between these two motions becomes higher.

Table 3 Dynamic properties of the first 11 modes for the bridge

Mode number	Natural frequency (Hz)	Mode description
1	0.1069	The 1st antisymmetric longitudinal floating of main girder
2	0.1893	The 1st antisymmetric vertical bending of main girder
3	0.2442	The 1st symmetric vertical bending of main girder
4	0.2734	The 1st symmetric lateral bending of main girder
5	0.3410	The 2nd symmetric vertical bending of main girder
6	0.4412	The vibration of main cables
7	0.4420	The 2nd antisymmetric vertical bending of main girder
8	0.4680	The vibration of main cables
9	0.4832	The vibration of main cables
10	0.4897	The vibration of main cables
11	0.5758	The 1st symmetric pitching of main girder

(a) mode 2

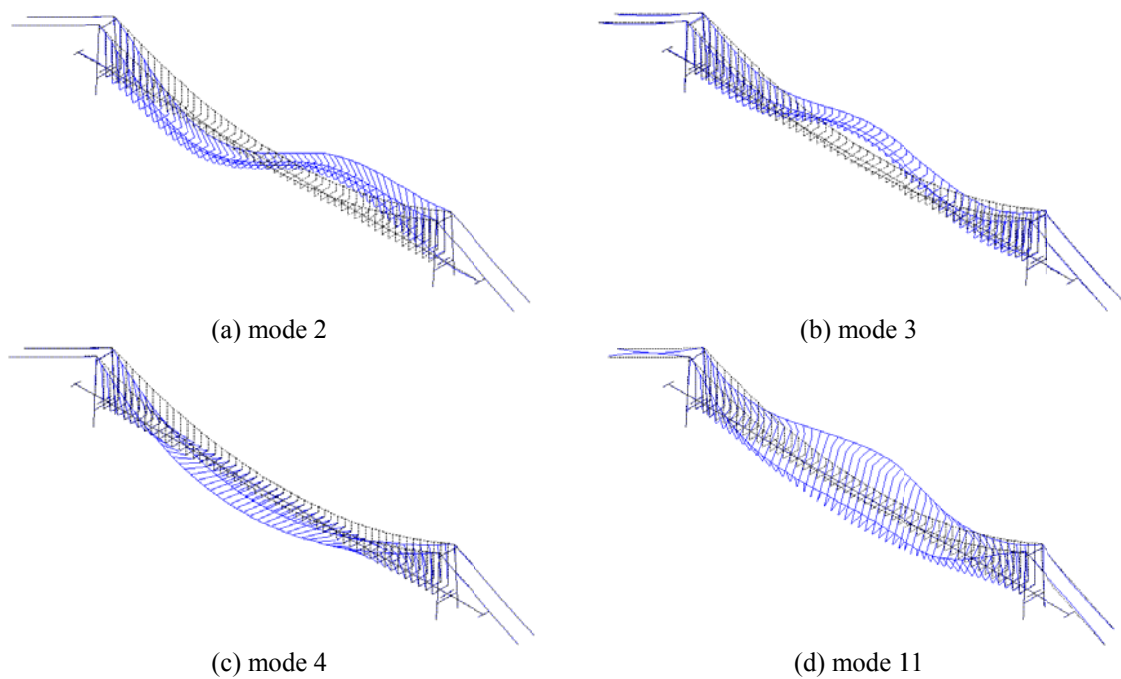(b) mode 3

(c) mode 4

(d) mode 11

Fig. 17 Main mode shapes

5. Aerodynamic stability analysis of the bridge

5.1 Flutter analysis of the bridge without considering the effect of vehicles

In this study, the nonlinear static analysis under the gravity loads is carried out first, followed by modal and then the flutter stability analysis on the bridge. Damped complex eigenvalue analysis is first carried out under wind velocities ranging from 0 to 130 m/s by assuming that the damping ratios ξ_j for all the first eleven modes are 0.5%. The proportionality coefficients α and β of Rayleigh damping matrix are obtained by the least square fitting as shown in Eq. (10). Fig. 18 shows the function values obtained from the assumed modal damping ratios and those reconstructed by use of the fitted proportionality coefficients. The conjugate pairs of complex eigenvalues and complex eigenvectors are obtained by the complex eigenvalue analysis. The first eleven conjugate pairs of complex eigenvalues and complex eigenvectors for Case 4 (i.e., without considering the presence of any vehicle) at $+3^{\circ}$ wind attack angle are extracted and the variation of the complex eigenvalues versus wind velocity is shown in Fig. 19.

It is found that the imaginary part of the complex eigenvalues for the first ten modes remains almost unchanged in the wind velocity range being studied, while the imaginary part of the complex eigenvalues for the eleventh mode, i.e. the torsional mode, gradually decreases with the increase of wind velocity. The real part of the complex eigenvalues for the bending modes decreases with the increase of wind velocity, while the real part of the complex eigenvalues for the torsional mode increases with the increase of wind velocity. The real part of the complex eigenvalues for other modes remains almost unchanged in the wind velocity range being considered. As shown in Fig. 19(a), the real part of the 11th complex mode becomes zero at the wind velocity of 118.1 m/s, and the corresponding imaginary part of the complex eigenvalue becomes 0.4885 Hz, indicating the onset of the flutter instability.

Table 4 lists the flutter wind velocities and flutter frequencies for Case 4 at 0°, $+3^{\circ}$ and -3° wind attack angles predicted by the present procedure.
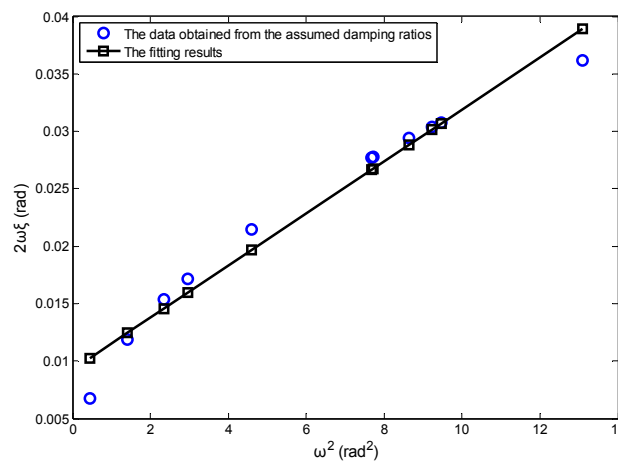

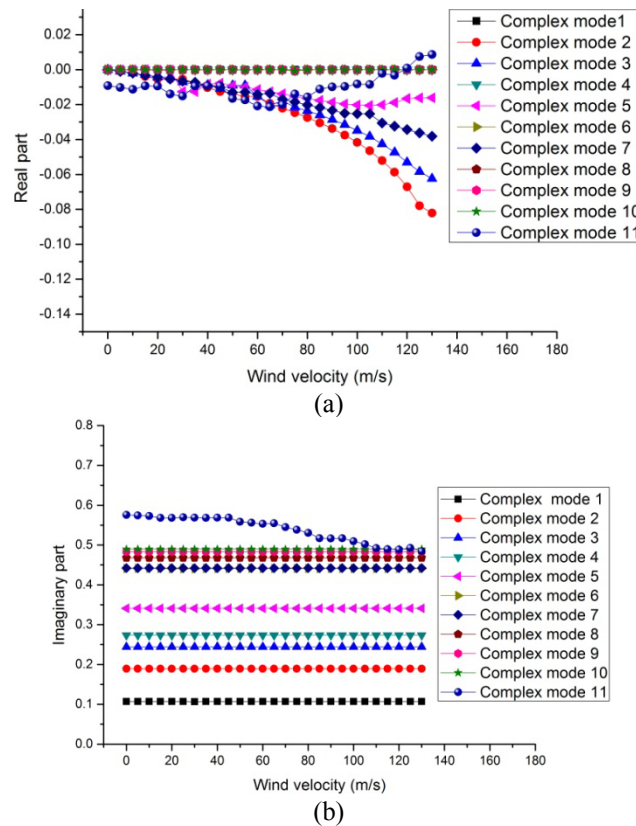Fig. 18 Least square fitting of proportionality coefficients

(a)

(b)

Fig. 19 Variation of complex eigenvalues versus wind velocity for Case 4 at +3° wind attack angle: (a) real part; (b) imaginary part

Table 4 Flutter analysis results for Case 4

Wind attack angles	Flutter wind velocity (m/s)	Flutter frequency (Hz)
0°	128.2	0.4680
+3°	118.1	0.4885
-3°	132.4	0.4559

From Table 4, it is found that the minimum flutter velocity occurs at +3° wind attack angle and the maximum flutter velocity occurs at -3° wind attack angle. The results suggest that it is relatively easier for the bridge to experience the aerodynamic instability under +3° wind attack angle, while more difficult under -3° wind attack angle. As shown in Fig. 4, for +3° wind attack angle, the flutter derivative A_2^* becomes negative at 0° and -3° wind attack angles and positive at +3° wind attack angle. With a larger negative value of A_2^* at -3° wind attack angle than 0° wind attack angle, the results show that the bridge may have the minimum flutter velocity for +3° wind attack angle and the maximum flutter velocity for -3° wind attack angle.

5.2 Flutter analysis of the bridge considering the effect of vehicles

To investigate the effect of vehicles on the flutter stability of the bridge, the flutter analysis is carried out using the identified flutter derivatives considering the effect of vehicles, as shown in Figs. 3~10. Table 5 lists the flutter wind velocities and flutter frequencies for Cases1, 2, and 3, corresponding to free flow, moderate flow, and busy flow, at 0°, +3° and -3° wind attack angles, respectively. For comparison purpose, the results for Case 4, i.e., "no vehicle on the bridge", are also listed in Table 5. Fig. 20 shows the comparison of flutter wind velocity of flutter analysis results.

Table 5 Flutter analysis results of Cases1, 2, and 3 comparing with Case 4

	Flutter wind velocity (m/s)				Percentage δ_v (%)		
	Case 1	Case 2	Case 3	Case 4	Case 1	Case 2	Case 3
-3°	135.3	137.2	133.1	132.4	2.19	3.63	0.53
0°	125.2	124.3	126.2	128.2	-2.34	-3.04	-1.56
+3°	121.3	123.4	125.2	118.1	2.71	4.49	6.01
	Flutter frequency (Hz)				Percentage δ_f (%)		
	Case 1	Case 2	Case 3	Case 4	Case 1	Case 2	Case 3
-3°	0.4529	0.4448	0.4541	0.4559	-0.66	-2.43	-0.39
0°	0.4770	0.4758	0.4814	0.4680	1.92	1.67	2.56
+3°	0.4870	0.4840	0.4860	0.4885	-0.31	-0.92	-0.51

Note: percentage δ_v=100×(flutter wind velocity for Cases 1, 2, 3 - flutter wind velocity for Case 4)/ flutter wind velocity for Case 4; and percentage δ_f=100×(flutter frequency for Cases 1, 2, 3 - flutter frequency for Case 4)/ flutter frequency for Case 4
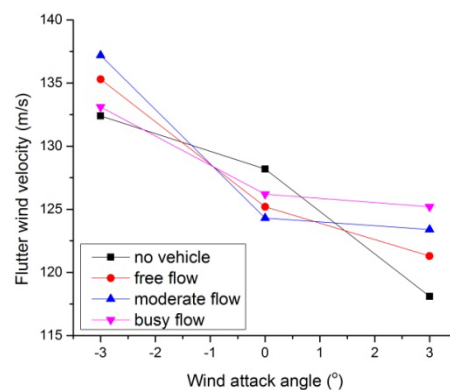

Fig. 20 Comparison of flutter wind velocity of flutter analysis results

From Table 5 and Fig. 20, it can be seen that the flutter wind velocities for all cases decrease with the increase of wind attack angle. The effect of vehicles on the flutter wind velocity is obvious. At 0° wind attack angle, the presence of vehicles results in the decrease of the flutter wind velocity, while it increases the flutter wind velocity at -3° and $+3^o$ wind attack angles. The effect of vehicles on the flutter wind velocity agrees well with that on the aerodynamic derivative A_2^* discussed above. More detailed discussions of the vehicles on the flutter derivatives are seen Han et al. (2014). From Table 5, it is also observed that the higher the flutter wind velocity is, the smaller the flutter frequency will be.

6. Conclusions

In this study, the flutter derivatives of the typical streamlined cross-section for a long-span suspension bridge considering different traffic flows were experimentally investigated. With the data of flutter derivatives, the sensitivity analysis of the vehicle distribution was conducted. With the identified flutter derivatives, the influence of vehicles on the flutter stability of the suspension bridge is investigated using the commercial FE package ANSYS. Based on the present study, the conclusions are summarized as follows:

(1) The influence of vehicles on the flutter derivatives of the typical streamlined cross-section cannot be ignored. Based on the results of the aerodynamic derivative A_2^*, the presence of vehicles on the bridge with 0° attack angle is disadvantageous to the aerodynamic stability of the bridge, while being advantageous at $+3^o$ and -3° attack angles.

(2) From the sensitivity analysis of the vehicle distribution on the aerodynamic derivative A_2^*, it is found that the vehicle distribution has small influence on the flutter derivatives. In the flutter stability analysis the effect of the vehicle distribution can be ignored.

(3) The effect of vehicles on the flutter wind velocity is obvious. The presence of vehicles results in a decrease of the flutter wind velocity at 0° wind attack angle, while an increase at -3° and $+3^o$ wind attack angles.

(4) It is found that the trends of the effects from the vehicle presence on the flutter wind velocity agree well with those on the aerodynamic derivative A_2^*, underlying the critical role of A_2^* in the flutter stability of streamlined bridge cross-sections.

Acknowledgements

References

Agar T.J.A. (1989), "Aerodynamic flutter analysis of suspension bridges by a modal technique", *Eng. Struct.*, **11**(2),75-82.

Cai, C.S., Albrecht, P. and Bosch, H.R. (1999). "Flutter and buffeting analysis: finite element and RPE solution", *J. Bridge Eng. - ASCE*, **4**(3), 174-180.

Cai, C.S. and Chen, S.R. (2004), "Framework of vehicle-bridge-wind dynamic analysis", *J.Wind Eng. Ind. Aerod.*, **92** (7-8), 579-607.

Chen, S.R., Cai, C.S. and Walshon, B. (2009), "From normal operation to evacuation: single-vehicle safety under adverse weather, topographic and operational conditions", *Nat. Hazards Rev. - ASCE*, **10**(2), 68-76.

Chen, S.R. and Wu, J. (2011), "Modeling stochastic live load for long-span bridge based on microscopic traffic flow simulation", *Comput. Struct.*, **89**(9-10), 813-824.

Chen, X. (2007), "Improved understanding of bimodal coupled bridge flutter based on closed-form solution", *J. Struct. Eng. – ASCE*, **133**(1), 22-31.

Chen, Z.Q., Han, Y., Hua X.G. and Luo, Y.Z. (2009), "Investigation on influence factors of buffeting response of bridges and its aeroelastic model verification for Xiaoguan Bridge", *Eng. Struct.*, **31**, 417-431.

Ding, Q., Chen, A. and Xiang, H. (2002), "Coupled flutter analysis of long-span bridges by multimode and full-order approaches", *J. Wind Eng. Ind. Aerod.*, **90**(12-15), 1981-1993.

Dung, N.N., Miyata, T., Yamada, H. and Minh, N.N. (1998), "Flutter responses in long span bridges with induced displacement by the mode tracing method", *J. Wind Eng. Ind. Aerod.*, **77-78**, 367-379.

Ge, Y.J. and Tanaka, H. (2000). "Aerodynamic stability of long-span suspension bridges under erection", *J. Struct. Eng. - ASCE*, **126**(12),1404-1412.

Han, Y. (2007), *Study on complex aerodynamic admittance functions and refined analysis of buffeting response of bridges*, Ph.D. thesis, China: Hunan University.

Han, Y., Liu, S., Hu, J.X., Cai, C.S., Zhang, J. and Chen, Z. (2014), "Experimental study on aerodynamic derivatives of a bridge cross-section under difference traffic flows", *J. Wind Eng. Ind. Aerod.*, **133**, 250-262.

Hua, X.G., Chen, Z.Q., Ni, Y.Q. and Ko, J.M. (2007), "Flutter analysis of long-span bridges using ANSYS", *Wind Struct.*, **10**(1), 61-82.

Jain, A., Jones, N.P. and Scanlan, R.H. (1996), "Coupled flutter and buffeting analysis of long-span bridges", *J. Struct. Eng. - ASCE*, **122**(7),716-725.

Katsuchi, H., Jones, N.P. and Scanlan, R.H. (1999), "Multimode coupled flutter and buffeting analysis of the Akashi-Kaikyo Bridge", *J. Struct. Eng. - ASCE*, **125**(1), 60-70.

Miyata, T. and Yamada, H. (1990), "Coupled flutter estimate of a suspension bridge", *J. Wind Eng. Ind. Aerod.*, **33**,341-348.

Namini, A. (1991), "Analytical modeling of flutter derivatives as finite elements", *Comput. Struct.*, **41**(5),1055-1064.

Namini, A., Albrecht, P. and Bosch, H. (1992), "Finite element-based flutter analysis of cable-suspended bridges", *J. Struct. Eng. - ASCE*, **118**(6), 1509-1526.

Niu, H.W., Chen, Z.Q. and Hua, X.G. (2007), "A novel 3-DOF forced vibration system for identification of eighteen flutter derivatives", *Proceedings of the 12th International Conference on Wind Engineering*, Cairns, Australia.

Niu, H.W., Chen, Z.Q., Liu, M.G., Han, Y. and Hua, X.G. (2011), "Development of the 3-DOF forced vibration device to measure the aerodynamic forces on section models", *Proceedings of the 13th International Conference on Wind Engineering*, Amsterdam, the Netherlands.

Scanlan, R.H. and Tomko, J.J. (1971), "Airfoil and bridge deck flutter derivatives", *J. Eng. Mech. - ASCE*, **97**(6),1717-1737.

Scanlan, R.H. (1978), "Action of flexible bridges under wind, I: flutter theory", *J. Sound Vib.*, **60**(2), 187-199.

Scanlan, R.H. and Jones, N.P. (1990), "Aeroelastic analysis of cable-stayed bridges", *J. Struct. Eng. - ASCE*

116(2), 279-297.

Tanaka, H., Yamamura, N. and Tatsumi, M. (1992), "Coupled mode flutter analysis using flutter derivatives", *J. Wind Eng. Ind. Aerod.*, **42**(1-3), 1279-1290.

Xie, J. and Xiang, H.F. (1985), "State-space method for 3-D flutter analysis of bridge structures", *Proceedings of the 1st Asia Pacific Symposium on Wind Engineering*, India.

Zhang, X.J. and Sun, B.N. (2004), "Parametric study on the aerodynamic stability of a long-span suspension bridge", *J. Wind Eng. Ind. Aerod.*, **92**(6), 431-439.